Optimized Skeletal Models of Butane Combustion

Y.X. Xin [1,*], D. Sheen[2], H. Wang [3], C.K. Law [1]

[1] Department of Mechanical and Aerospace Engineering
Princeton University, Princeton, NJ 08544, USA
[2] Chemical Sciences Division,
National Institute of Standards and Technology, Gaithersburg, MD 20899, USA
[3] Department of Aerospace and Mechanical Engineering
University of Southern California, Los Angeles, California 90089, USA

Abstract

Skeletal reaction models for *n*-butane and *iso*-butane combustion are derived from the detailed gas phase chemistry model of USC Mech II through directed relation graph (DRG) and DRG aided sensitivity analysis (DRGASA) methods. The skeletal models generated from various combustion systems, e.g. auto-ignitions versus premixed flames, *n*-butane versus *i*-butane, are compared, and analyzed based on the temperature and species profiles during ignition and within the flames. The reduced models are further optimized through the method of uncertainty minimization by polynomial chaos expansion (MUM-PCE) to enhance model performances. The uncertainty of the optimized model is quantified by the spectral expansion technique, exploring the relationship between the model size and uncertainty.

Keyword: model reduction, model optimization, uncertainty quantification

* Corresponding author: yxin@princeton.edu

1. Introduction

Detailed reaction models are widely employed in predicting combustion phenomena (Lu and Law 2009). The development of detailed models usually starts from a compilation of a set of elementary reactions whose rate parameters are derived from experimental rate measurements, reaction rate theory, or, in many cases, estimations from analogous reactions. The model predictiveness may be improved by a multi-parameter optimization. Examples include the solution mapping coupled with constrained global optimization within rate parameter uncertainties (Frenklach 1984; Frenklach et al. 1992).

With the increases of fuel complexity, the model size expands from around 10 species for hydrogen (e.g., Davis et al. 2005) to thousands species for *n*-hexadecane (e.g., Westbrook et al. 2009). The large size limits the practical usability of these models in computational fluid dynamics simulations. A variety of model reduction strategies have been proposed (see, e.g., Tomlin et al. 1998; Frenklach 1991; Law et al. 2003). In general, the methods of model reduction may be categorized into skeletal reduction and time scale analysis. Skeletal reduction eliminates unimportant species and reactions, which can be achieved by sensitivity analysis (Rabitz et al. 1983; Turanyi 1990; Tomlin et al. 1997), principal component analysis (Vajda et al. 1985), Jacobian analysis (Turanyi 1990), optimization (Bhattacharjee et al. 2003), detailed reduction (Wang & Frenklach 1991), directed relation graph (DRG) (Lu & Law 2005, 2006 a&b), DRG with error propagation (DRGEP) (Pepiot-Desjardins & Pitsch 2008), and DRG-aided sensitivity analysis (DRGASA) (Sankaran et al. 2007; Zheng et al. 2007). A time-scale analysis identifies fast species as well as reactions, and describes their time evolution by algebraic equations. Methods of time-scale analysis are based on primarily quasi-steady-state (QSS) and partial equilibrium (PE) assumptions (Peters & Williams 1987; Chen 1988; Sung et al. 2001; Lovas et al. 2000; Soyhan et al. 2002). Several approaches to identifying the QSS species have been proposed (Lovas et al. 2000; Soyhan et al. 2002; Mendiara et al. 2004; Massias et al. 1999a&b; Lu et al. 2001; Montgomery et al. 2006; Lu & Law 2008). Other, and perhaps more systematic approaches to time-scale analysis include intrinsic low-dimensional manifolds (ILDM) (Maas & Pope 1992) and computational singular perturbation (CSP) (Lam & Goussis 1988, 1994; Valorani et al. 2003&2006).

One of the objectives of the present study is to propose an improved model reduction strategy by integrating the processes of skeletal reduction and model optimization: the derived skeletal model is subject to optimization to improve its predictiveness. Historically, the accuracy of a reduced model is ensured typically by comparing its predictions against those of the detailed model (Law et al. 2003; Wang and Frenklach 1991; Lovas et al. 2000), the uncertainty of the reduced model has been rarely discussed. Thus, the second objective of the current work is to address this issue by examining uncertainties of skeletal models by exploring the correlation between the model size and uncertainty. A prototypal detailed

chemistry model, USC Mech II, (Wang et al. 2007) is used for this purpose with *n*-butane and *i*-butane combustion illustrated as examples.

2. Methodology

2.1 Skeletal Model Reduction

A detailed reaction model is composed of three types of species: nonessential ones, critical ones, and marginal ones. A successful skeletal reduction eliminates all nonessential species, retain all critical ones, while properly deal with marginal ones. The importance of species can be assessed through an analysis of the species conversion flux, which includes DRG (Lu & Law 2005, 2006a&b), DRGEP (Pepiot-Desjardins & Pitsch 2008), and sensitivity analysis (Rabitz et al. 1983; Turanyi 1990; Tomlin et al. 1997). The two strategies have their respective advantages and disadvantages. The flux method is computationally affordable and able to identify nonessential species efficiently. However, the method can misestimate the importance of marginal and critical species. The sensitivity method quantifies the importance of species with better accuracy but it can have prohibitive computational costs, preventing its application for large models. Currently, skeletal model reduction is conducted in two steps (Zheng et al. 2007): the detailed model is first reduced by an importance-estimated method to an intermediate skeletal model, which is reduced further to a final skeletal model by an importance-computed method. This two-step strategy is adopted here by combining DRG with DRGASA.

Both methods have been discussed in details elsewhere (Lu & Law 2005, 2006a & 2006b; Zheng et al. 2007). They are briefly discussed here. DRG represents the chemistry model by directed relation graph, whose nodes are species and the width to edge from node A to B, r_{AB}, is calculated as:

$$r_{AB} = \frac{\sum\limits_{i=1,n_R} \left| \nu_{i,A} \omega_i \delta_B^i \right|}{\sum\limits_{i=1,n_R} \left| \nu_{i,A} \omega_i \right|} \# \tag{1}$$

where

$$\delta_B^i = \begin{cases} 1, & \text{if the } i\text{-th reaction involves species B} \\ 0, & \text{otherwise} \end{cases},$$

subscripts A and B indicate the species identity, n_R is the total number of reactions, $\nu_{i,A}$ is the stoichiometric coefficient of species A in the i th reaction, ω_i is the net reaction rate of the i th reaction. The value of r_{AB} quantifies the importance of species B to A. The skeletal

reduction is conducted by truncating the edges narrower than the user-specified threshold, ε, and the resulting graph maps to the skeletal model. Species are gradually eliminated with increasing ε, and the critical ε value responding to the reduction of a certain species qualitatively indicates the importance of this species to the model. In the current work, species with ε, > 0.5 are excluded from the subsequent sensitivity test. The species are ranked by their impacts on predicting a prescribed set of global combustion responses, allowing model reduction to be carried out successively, until the model cannot satisfy a prescribed accuracy requirement.

2.2 Mechanism Optimization

The purpose of DRGASA is to ensure that reaction pathways necessary to describe a set of combustion phenomena are retained in the reduced model. Removal of reaction pathways can lead to quantitative changes in model prediction. Because the dimensionality of the reduced model generally remains to be large, it should be possible to constrain the reduced model against the detailed model by an error minimization procedure. Rate coefficients subject to the minimization procedure are selected using a one-at-a-time sensitivity analysis, as was discussed in Sheen and Wang (2011b). For each computational experiment the uncertainty-weighted sensitivity coefficient $S_{r,k}$ may be defined as,

$$S_{r,k} = (d\ln\eta_r/d\ln A_i)\ln f_i \tag{2}$$

where η_r is the response, A_i and f_i are the Arrhenius prefactor and the uncertainty factor of the i th reaction. The active rate parameters are selected here as those with $S_{r,k} > \max(S_{r,k})/10$.

Ignition delay time simulations were performed using a kinetic integrator based on the DVODE solver (Brown et al. 1989), using the chemical production terms provided by Sandia CHEMKIN-II (Kee et al. 1989). Laminar flame speed was computed using Sandia PREMIX (Kee et al. 1986a) and TRANSPORT (Kee et al. 1986b), with modifications from Middha & Wang (2005).

Model constraint uses the method of uncertainty analysis using polynomial chaos expansions (MUM-PCE) (Sheen and Wang 2011b), which is summarized here. It is assumed that the uncertain parameters in the model can be expressed as a random vector $\mathbf{X} = \mathbf{x}^{(0)} + \mathbf{x}^{(1)}\xi$, where $\mathbf{x}^{(0)}$ is the factorial variable vector whose elements are

$$x_i^{(0)} = \frac{\ln\theta_i/\theta_{i,0}}{\ln f_i} \# \tag{3}$$

where θ_i is the ith active parameter and $\theta_{i,0}$ its nominal value. ξ is a vector of independent, identically distributed normal random variables with mean 0 and variance 1, and $\mathbf{x}^{(1)}$ is a

transformation matrix, so that $\mathbf{X}$ follows a multivariate normal distribution with mean $\mathbf{x}^{(0)}$ and covariance matrix $\Sigma = \mathbf{x}^{(1)}\mathbf{x}^{(1)T}$.

MUM-PCE applies Bayes' Theorem to determine the joint probability density function (PDF) of the active parameters, which results in the following PDF for the constrained rate parameters,

$$\ln P_\mathbf{X}(\mathbf{x}) \sim -\left[\sum_{r=1}^{N_e}\left(\frac{\eta_r(\mathbf{x})-\eta_r^{\mathrm{det}}}{\sigma_r}\right)^2 + \sum_{i=1}^{N_r}4x_i^2\right] \# \tag{4}$$

Here, $\eta_r(\mathbf{x})$ is the model prediction as a function of the rate parameters $\mathbf{x}$, N_e is the number of computational experiments and N_r the number of active variables. η_r^{det} is the detailed model prediction, and σ_r is the error tolerance between the detailed and reduced model predictions. This is taken to be 2 cm/s for laminar flame speeds and 0.2 in the natural logarithm of ignition delay time in microsecond, which is comparable to the experimental uncertainty.

Eq. 3 can be approximated by a multivariate normal distribution, which will then have an $\mathbf{x}^{(0)*}$ that in some sense best reproduces the detailed model, and a Σ^* that best reproduces their uncertainty. $\mathbf{x}^{(0)*}$ is found by finding the mode of the PDF in Eq. 3, equivalent to the least-squares optimization problem

$$\mathbf{x}^{(0)*} = \arg\max_\mathbf{x} \ln P_\mathbf{X}(\mathbf{x}) \# \tag{5}$$

which is solved using the LMDIF solver in the MINPACK library (More et al. 2012). Σ^* is found by linearizing the model predictions in the vicinity of $\mathbf{x}^{(0)*}$, which yields

$$\Sigma^* = \left(\sum_{r=1}^{M}\frac{\mathbf{J}_r\mathbf{J}_r^T}{(\sigma_r)^2} + 4\mathbf{I}\right)^{-1} \# \tag{6}$$

where $\mathbf{J}_r$ is the gradient of $\eta_r(\mathbf{x}^{(0)*})$. To reduce the computational complexity of Eqs. 4 and 5, the method of solution mapping (Frenklach 1984; Frenklach et al. 1992) is used, in which model predictions are expressed as polynomials with respect to the reaction rate parameters, $\eta_r(\mathbf{X}) = \mathbf{X}^T\mathbf{b}_r\mathbf{X} + \mathbf{a}_r^T\mathbf{X} + \eta_0$, where $\mathbf{a}_r$ and $\mathbf{b}_r$ are the first and second derivatives of η_r. The derivatives are calculated using the sensitivity-analysis-based method (SAB) (Davis et al. 2004). Then $\mathbf{J}_r = 2\mathbf{b}_r\mathbf{x}^{(0)*} + \mathbf{a}_r$.

It is possible that the model will be reduced to the point that it will not be possible to reproduce the detailed model prediction within the error tolerance for all conditions. To

identify these conditions, the MUM-PCE consistency analysis is used. In this procedure, the consistency criterion is defined as

$$\mathcal{F}_r = \left| \frac{\eta_r \left(\mathbf{x}^{(0)*} \right) - \eta_r^{\text{det}}}{\sigma_r} \right| \# \tag{7}$$

If $\mathcal{F}_r > 1$, then the rth reduced model prediction is inconsistent. If more than one prediction is inconsistent, then a strength function S_r is defined

$$S_r = \left| \frac{\mathbf{J}_r^T \mathbf{x}^{(0)*}}{\|\mathbf{J}_r\| \|\mathbf{x}^{(0)*}\|} \right| \# \tag{8}$$

which is the normalized scalar product between the posterior model vector and the model response gradient $\mathbf{J}_r$. The condition that has the largest $W_r = \mathcal{F}_r S_r$ is removed from consideration and a new constrained model is determined; the procedure is iterated until all remaining reduced and detailed model predictions are consistent with each other.

2.3 Uncertainty Quantification

Uncertainty in the reduced model predictions is calculated by propagating the random-variable expression for $\mathbf{X}$ through the polynomial expression $\eta_r \left(\mathbf{X} \right) = \eta_r \left(\mathbf{x}^{(0)} \right) + \mathbf{J}_r^T \mathbf{x}^{(1)}$; the uncertainty in the reduced model prediction is then equal to $\mathbf{J}_r^T \Sigma \mathbf{J}_r$. For models that are relatively detailed, the uncertainty should increase with increasing model complexity. In these cases, channels that are added back into the model contribute additional uncertainty to the model's predictions, but have a minimal effect on the principal channels. On the other hand, for models of low detail, the uncertainty might decrease with increasing model complexity. If a principal channel is removed in the reduction process, other principal channels become increasingly rate limiting. Although the removed channel no longer contributes any uncertainty, the increased sensitivity of the model prediction to the rates of the remaining channels more than compensates.

3. Skeletal Reduction

3.1 Skeletal Model

Combustion properties of n-butane- & i-butane-air mixtures are simulated using USC Mech II (Wang et al. 2007). USC Mech II is composed of 111 species and 784 reactions. This model was developed for high-temperature oxidation of H_2, CO and C_1-C_4 hydrocarbons. In the current study, auto-ignition delays and laminar flame speeds were chosen as the global response targets, while the thermodynamic space covers pressure from 1 to 20 atm, initial temperature from 800 to 1500K for auto-ignition, inlet temperature of 300 K for laminar premixed flame, and equivalence ratio from 0.6 to 1.5.

The skeletal reduction was conducted using DRG for four types of combustion responses: auto-ignition of *n*-butane, laminar premixed flames of *n*-butane, auto-ignition of *i*-butane and laminar premixed flames of *i*-butane. Within each category, the temperature and species concentrations were sampled from typical temporal moments of the auto-ignition process as well as spatial locations within the laminar premixed flame. Figure 1 presents the correlation between the number of species in the resulting skeletal model and the selection of a threshold value. In a previous study on *n*-heptane combustion using a substantially large detailed model (Lu & Law 2006b), a threshold value of 0.1 was shown to be a reasonable cutoff. In the current work, however, a threshold value of 0.1 can only remove around ten species, which indicates the compact structure of USC Mech II. As such, no species is directly eliminated by DRG analysis in this work, and the acquired knowledge further guides the skeletal reduction of DRGASA. Spanning all considered thermodynamic conditions, DRGASA calculates the maximal error in ignition delays and laminar flame speed caused by the removal of each individual species, and accordingly decides the priority of species to the model. Figure 2 shows the dependence of model error on the model size. By combining the information from auto-ignition and laminar premixed flame, three skeletal models with different levels of accuracy are generated, as shown in Table 1. The models of 49 species for *n*-butane and 54 species for *i*-butane are close to the detailed model in terms of their predictions within the condition tested. In contrast, the bad performances of other skeletal models are attributed to missing reaction pathways under certain circumstances.

Table 1. Summary and test results for skeletal models of *n*-butane & *i*-butane combustion.

Model	Number of species	Number of reactions	Relative error, %[a]	
			Ignition delay	Flame speed
nbut-1	49	384	27.6/6.3[b]	2.3/1.1[b]
nbut-2	43	309	60.4	3.8
nbut-3	31	152	100.0	11.1
ibut-1	54	402	24.7/6.4[b]	2.4/1.2[b]
ibut-2	47	343	61.3	5.0
ibut-3	38	233	100.0	12.6

[a] The reported relative error is selected as the worst case, calculated based on auto-ignition and premixed flame of *n*-butane and *i*-butane for pressures from 1 to 20 atm, initial temperature from 800 to 1500 K for auto-ignition, and initial temperature 300 K for premixed flame, and equivalence ratio from 0.6 to 1.5.
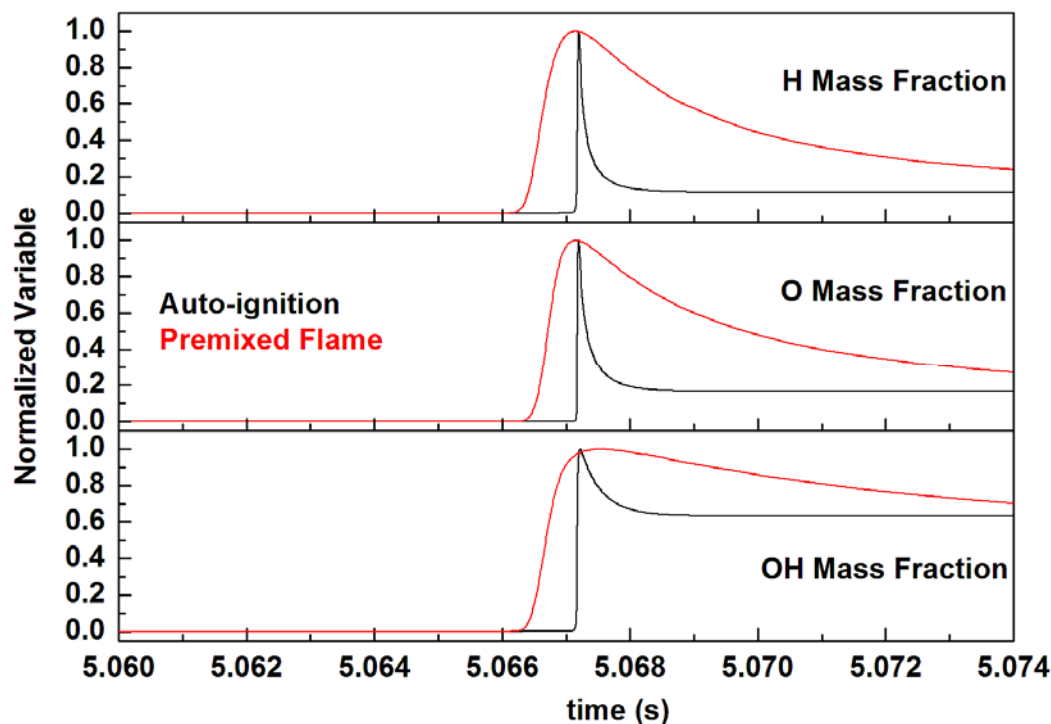[b] After optimization.
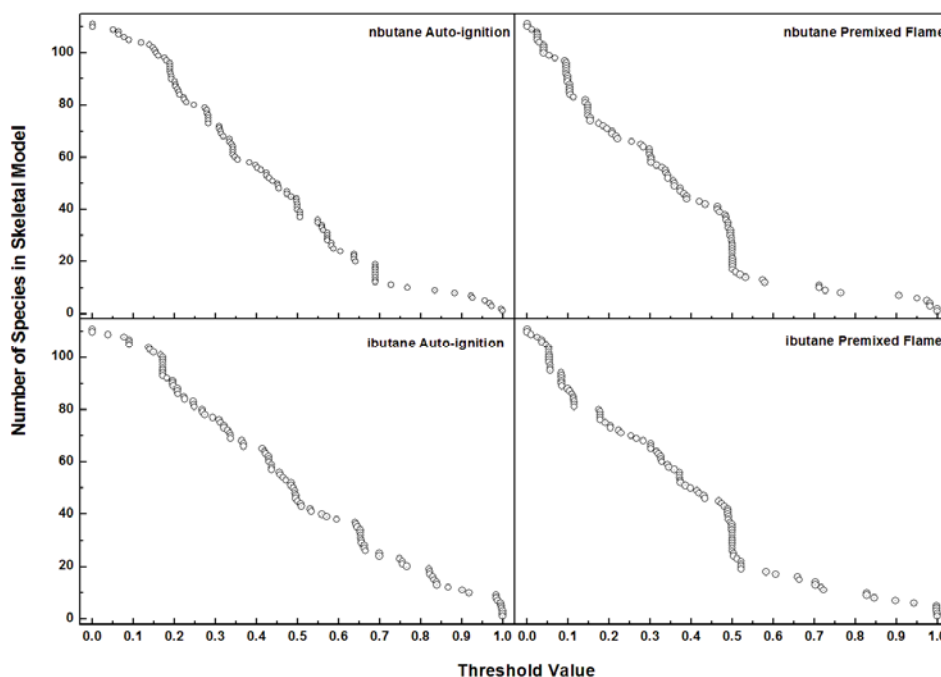
Figure 1. Dependence of number of species in a skeletal model on the threshold value for DRG, calculated based on auto-ignition and premixed flame of *n*-butane and *i*-butane for pressure from 1 to 20 atm, initial temperature from 800 to 1500 K for auto-ignition, and initial temperature 300 K for premixed flame, and equivalence ratio from 0.6 to 1.5.
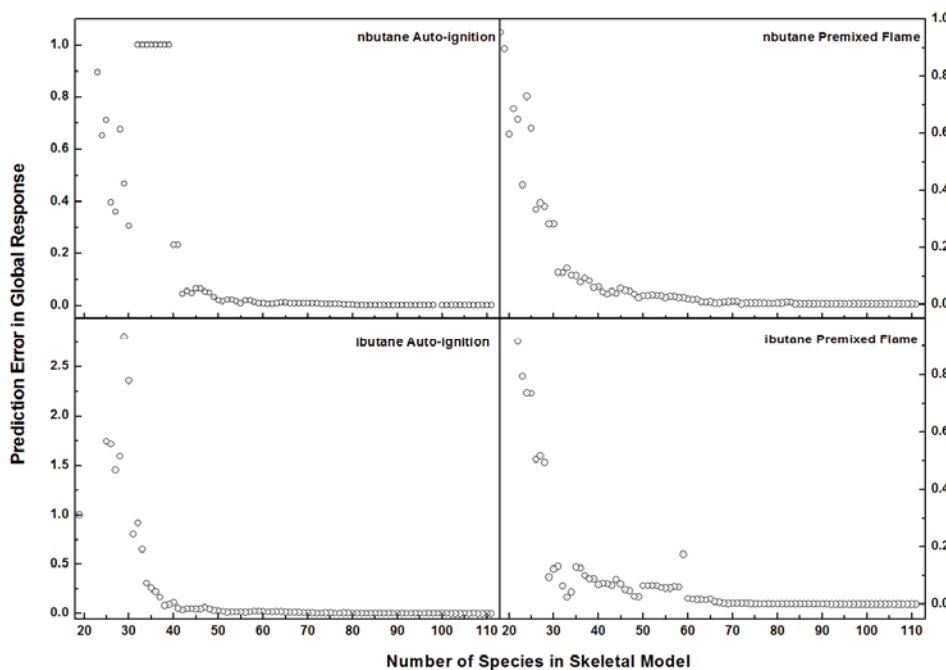
Figure 2. Dependence of relative prediction error in global responses on the number of species in skeletal model, calculated based on auto-ignition and premixed flame of *n*-butane and *i*-butane for pressure from 1 to 20 atm, initial temperature from 800 to 1500 K for auto-ignition, and initial temperature 300 K for premixed flame, and equivalence ratio from 0.6 to 1.5.

3.2 Model Reduction Analysis

The importance of various species is ranked by DRGASA, but the ranking may vary for different combustion processes. Therefore, the priority orders resulting from different cases, e.g., auto-ignition verse premixed flame, n-butane verse i-butane, reveal the essential chemistry properties of these systems. Models derived independently from auto-ignition and laminar premixed flame share over 90% species. For a skeletal model with 50 species, the species unique to auto-ignition are CH_3CCH_2, iC_3H_7, nC_4H_5, iC_4H_7, $CH_2CHCHCHO$ and those unique to flames are CH, CH_2OH, C_2H, H_2CC, CH_3CO. The similarity may be explained by the temperature and species profiles calculated for stoichiometric n-butane oxidation in auto-ignition and premixed flame at the atmosphere pressure. Figure 3 shows the time evolution of normalized temperature, mass fractions of n-C_4H_{10} and O_2. The flame propagation velocity used for spatial position and time conversion is 39.5 cm/s. Similar plots for key molecular intermediates, including C_3H_6, C_2H_4, CO and H_2, and free radicals H, O and OH are presented in Figure 4. It is seen that besides of n-butane, auto-ignition and premixed flame share the similar profiles in temperature, oxygen, key molecular intermediates and key free radicals. The different degrees of involvement of C_3-C_4 fragments are attributed to fuel decomposition unique to these two oxidation environments. In the premixed flame, the radicals generated in the high temperature region diffuse into the low temperature region and initiate fuel decomposition. In the induction period of auto-ignition, n-butane decomposes primarily through C_3-C_4 fragments with low radical concentrations. It is for this reason that the destruction rates of n-butane can be drastically different. Because of diffusion in premixed flames, the radical profiles become significantly broaden in comparison to auto-ignition. For skeletal models derived independently for auto-ignition of n-butane and i-butane, 80% of species retained are identical between the two models. For a 50-species model, the species unique to n-butane are nC_3H_7, C_3H_8, nC_4H_5, iC_4H_5, C_4H_8-2, pC_4H_9, sC_4H_9, C_4H_{10} and $CH_2CHCHCHO$ and those unique to i-butane are CH_2OH, CH_3CO, pC_3H_4, CH_2CHCO, CH_3COCH_3, iC_4H_9, tC_4H_9, iC_4H_{10} and C_6H_5 for i-butane. The two models share the same chemistry of small hydrocarbons (C_1-C_2), CO and H_2.
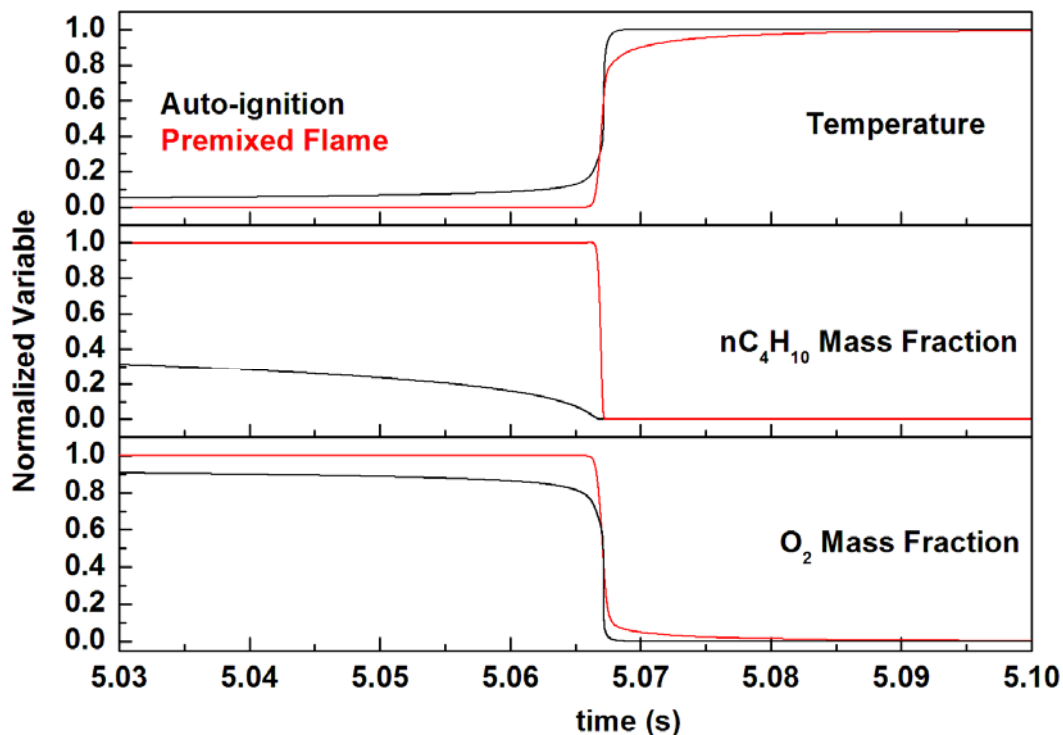
Figure 3. Profiles of temperature and reactants, calculated for auto-ignition at an initial temperature of 800 K and premixed flame of *n*-butane-air mixture at 300 K, all at 1 atm pressure and unity equivalence ratio.
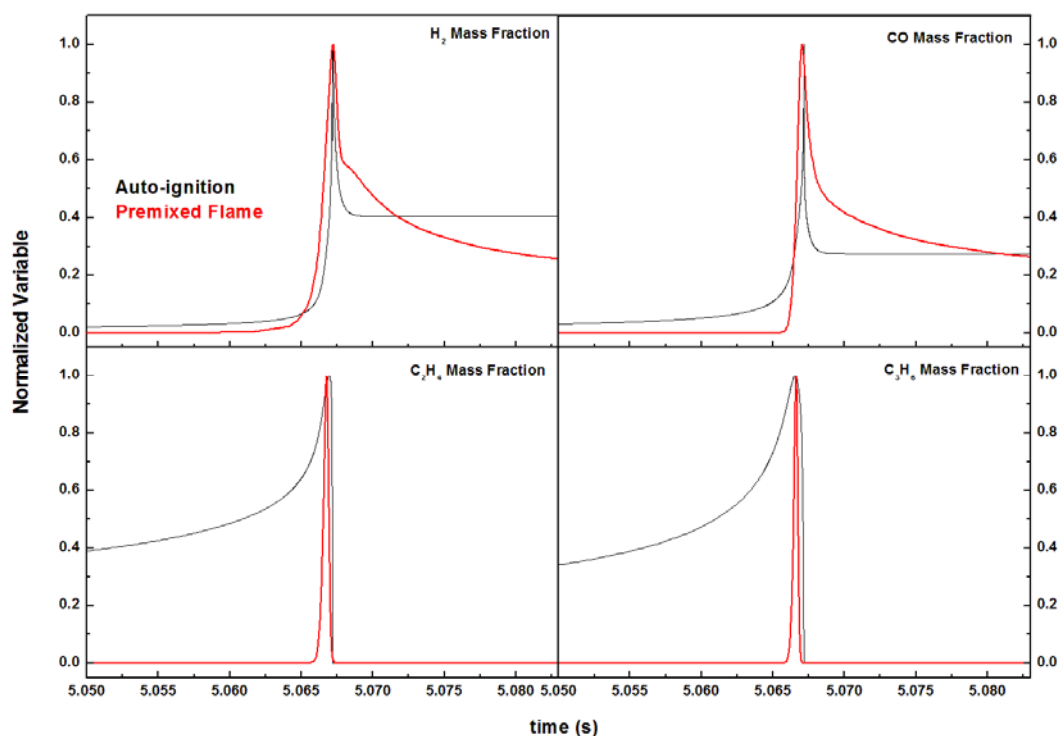
Figure 4 (a). Profiles of key molecular intermediates calculated for auto-ignition at an initial temperature of 800 K and premixed flame of *n*-butane-air mixture at 300 K, all at 1 atm pressure and unity equivalence ratio.

10

Figure 4 (b). Profiles of free radicals calculated for auto-ignition at an initial temperature of 800 K and premixed flame of *n*-butane-air mixture at 300 K, all at 1 atm pressure and unity equivalence ratio.

4. Optimization and Uncertainty Quantification of Skeletal Model

Skeletal models of 49 species for *n*-butane and 54 species for *i*-butane are constrained against the predictions of the detailed model in 54 combustion targets, including 45 ignition delay times and 9 flame speeds. They span the same range of thermodynamic conditions and stoichiometry where these skeletal models are derived. The predictions of the unconstrained and constrained skeletal models are compared to those of the full model, as shown in Figure 5. Clearly, the performances of the skeletal models are improved by the constraining process, which reduced the maximal error from 25% to 6% or ignition delay and from around 2 to 1% for the flame speeds. For *n*-butane and *i*-butane, the rate coefficients of 103 and 97 reactions are impacted by the constraining process. The changes in the A factors are presented in Figures 6 and 7 for *n*-butane and *i*-butane respectively. The perturbed rate coefficients are all within a factor of two from those in the detailed model. Model constraining for skeletal models of 43 and 31 species for *n*-butane and 47 and 38 species for *i*-butane was not attempted, because these models are known to have missing critical reaction pathways. Although their predictiveness can be improved for fixed test cases, their validity and generality cannot be determined.
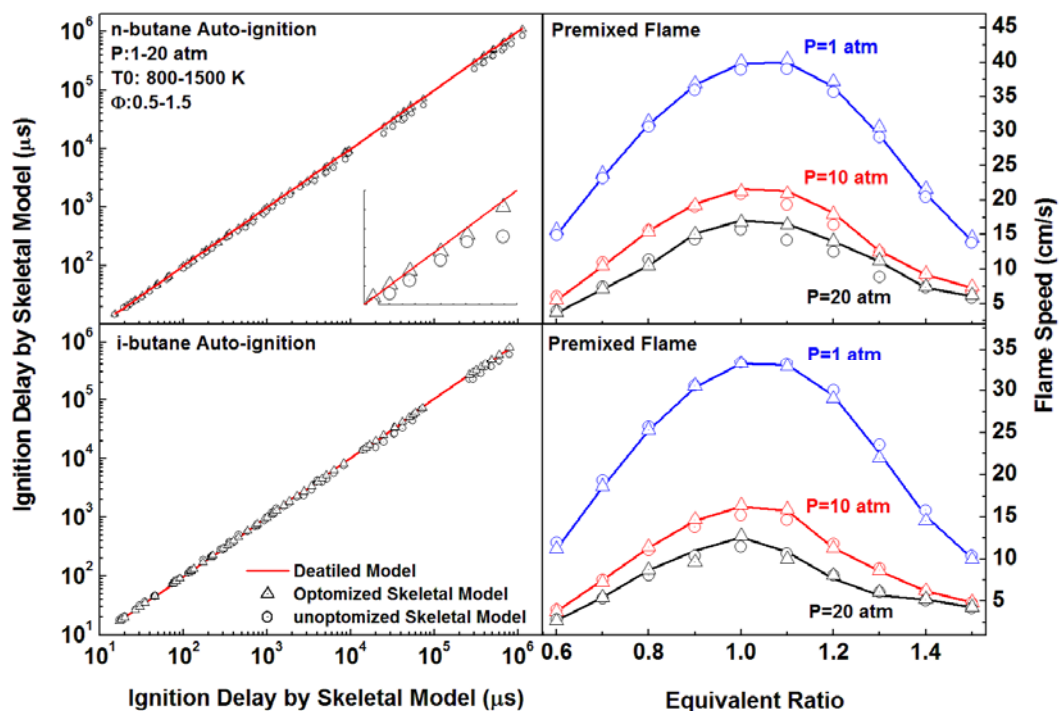
Figure 5. Ignition delay times (left panel) and flame speeds (right panel) predicted for butane-air mixtures. The *n*-butane and *i*-butane skeletal model contain 49 and 54 species, respectively.
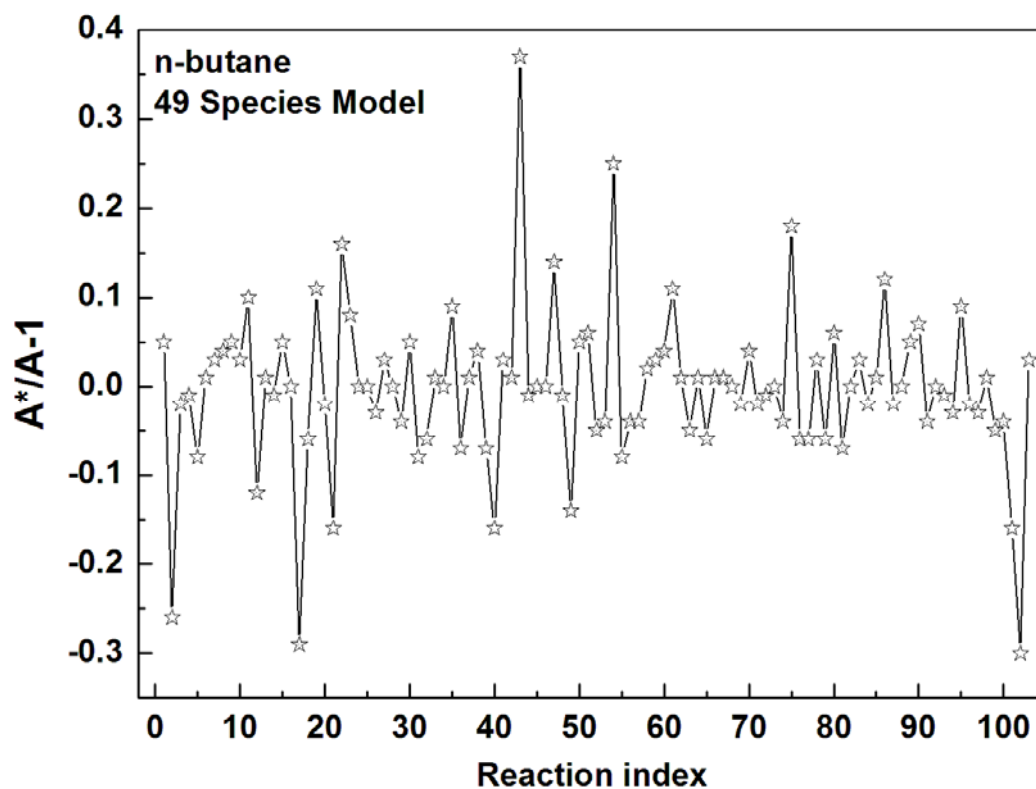

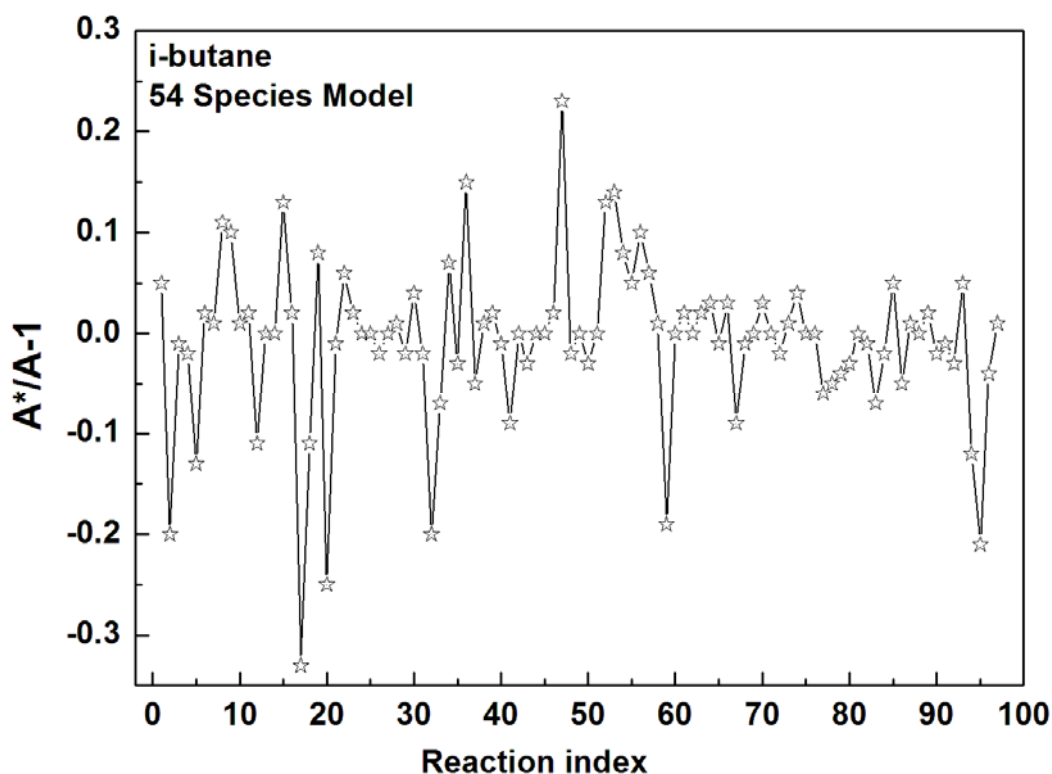**Figure 6**. Changes in the *A* factors in the constrained skeletal model of 49 species for *n*-butane.

Figure 7. Changes in the *A* factors in the constrained skeletal model of 54 species for *i*-butane.

The uncertainties of the skeletal models are presented in Figures 8 to 11, which show a non-monotonous relationship between model size and prediction uncertainty. Intuitively, the model uncertainty is expected to increases with the model size, because a larger model involves more rate parameters with intrinsic uncertainties, which naturally widens the uncertainty of the model. This understanding is supported by the high temperature auto-ignition of butane, and cannot account for situations in low temperature auto-ignition and premixed flames. We propose a hypothesis for this dilemma: the uncertainty of a model is not solely decided by its size but also depends on the completeness of the model. For a complete or nearly-complete model, which includes all major reactions, the further added pathways are minor channels, which slightly and randomly changes model prediction and uncertainty. Statistically, the influence of minor reaction pathways closes to be cancelled out, since the complexity of the model increases with the model size, the error bar of model prediction gently expands. In contrast, for an incomplete model, the further added pathway may significantly impact and even dominates model performances. It is impossible to predict the model uncertainty under this condition. Specifically for the case study in this paper, as well known in the combustion community, auto-ignition of high temperature process involves fewer reaction channels than low temperature auto-ignition and flame propagation, which implies the skeletal models are more complete for high temperature auto-ignition than other two scenarios.
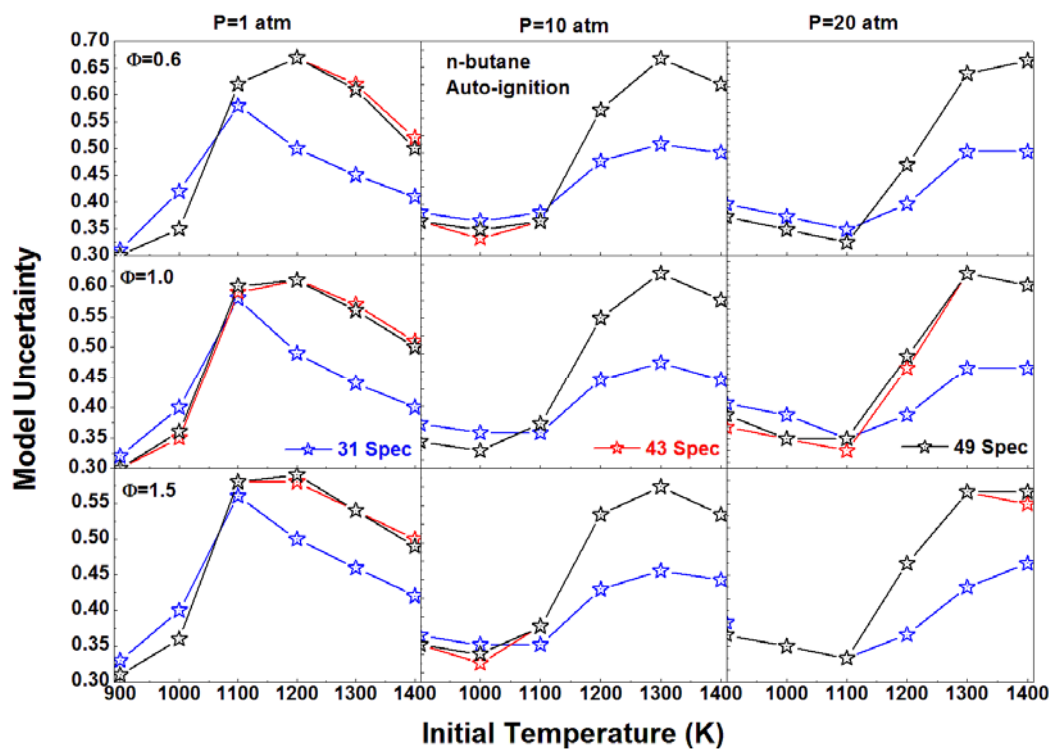
Figure 8. Uncertainty of skeletal models for *n*-butane in predicting ignition delay times.
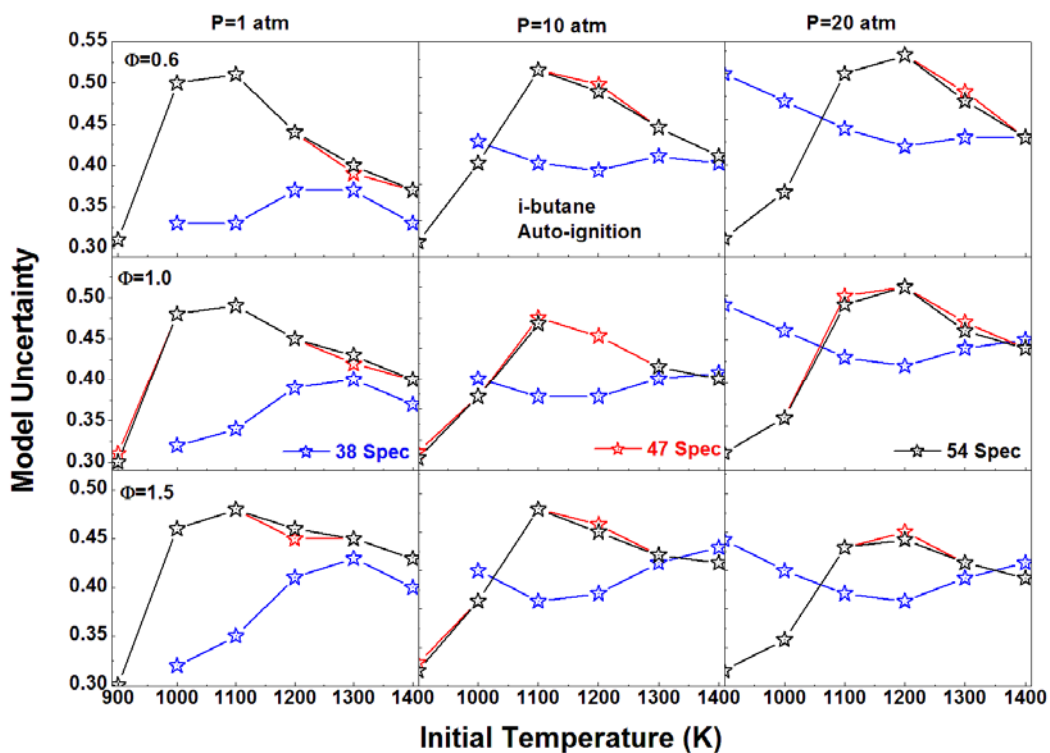

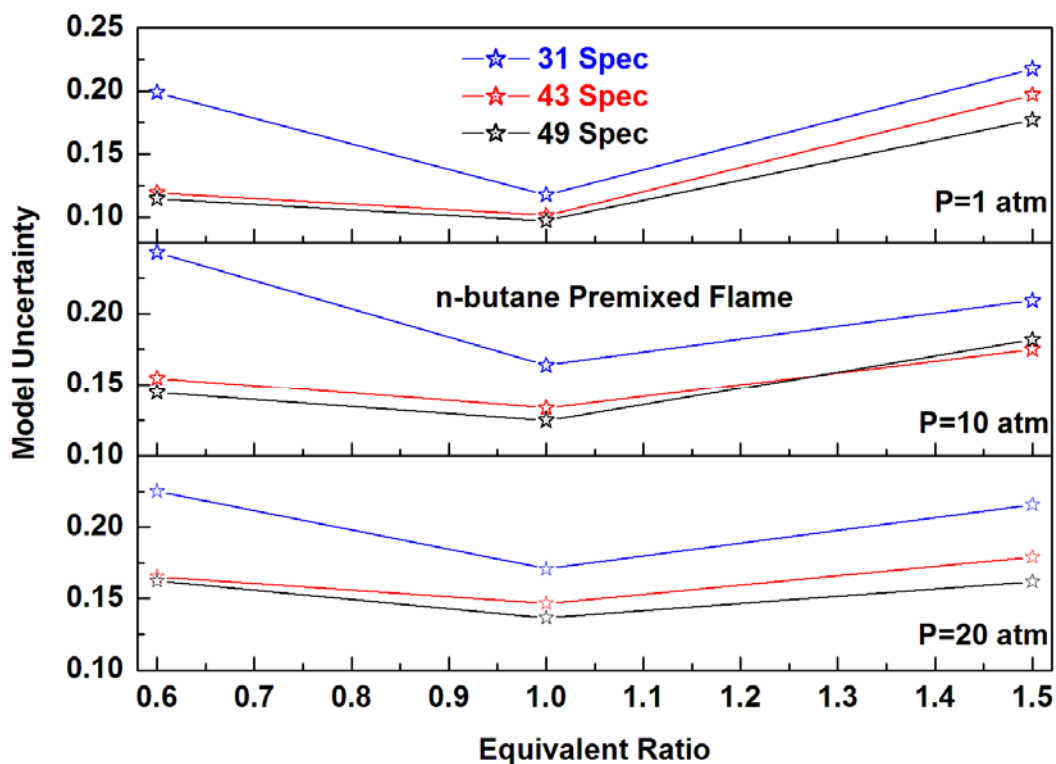**Figure 9**. Uncertainty of skeletal models for *i*-butane in predicting ignition delay times.

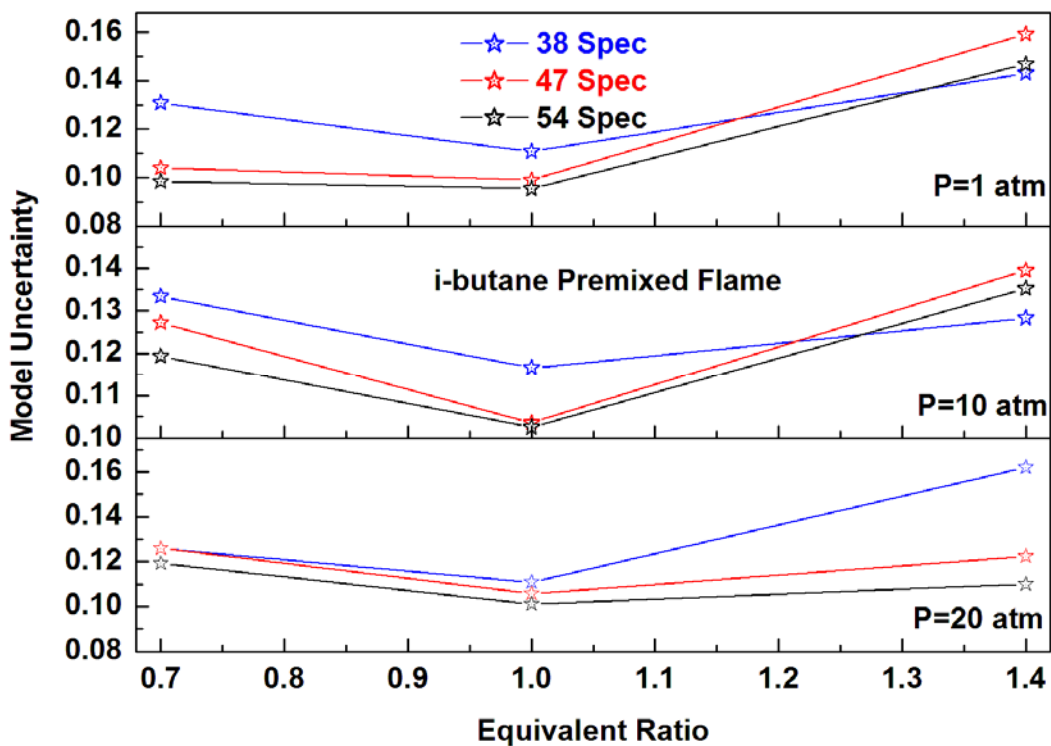**Figure 10**. Uncertainty of skeletal models for *n*-butane in predicting flame speeds.

Figure 11. Uncertainty of skeletal models for *i*-butane in predicting flame speeds.

5. Conclusions

Chemistry models for *n*-butane and *i*-butane combustion are derived from USC Mech II by skeletal reduction and model optimization. The yielded models reproduce the prediction of the detailed model. The rate coefficients of the skeletal model are adjusted systematically within their uncertainty bounds using MUM-PCE. The relationship between the model size and model prediction uncertainty is explored by quantifying the prediction uncertainty of skeletal models with different accuracies, which ends up a case dependent correlation: for a complete model, the uncertainty gently increases with the model size, while the uncertainty cannot be predicted for an incomplete model.

Reference

Bhattacharjee B., Schwer D.A., Barton P.I., Green W.H. (2003) Combust. Flame **135**, 191.

Chen J.Y. (1988) Combust. Sci. Technol. **57**, 89.

Brown P.N., Byrne G.D., Hindmarsh A.C., (1989) SIAM J. Sci. Stat. Comput. **10**, 1038.

Davis S.G., Joshi A.V., Wang H., Egolfopoulos F.N. (2005) Proc. Combust. Inst. **30**, 1283.

Davis S.G., Mhadeshwar A.B., Vlachos D.G., Wang H., (2004) Int. J. Chem. Kinet. **36**, 94.

Frenklach M. (1984) Combust. Flame **58**, 69.

Frenklach M. (1991) Reduction of Chemical Reaction Models; American Institute of Aeronautics and Astronautics Inc,

Frenklach M., Wang H., Rabinowitz M.J. (1992) Prog. Energy Combust. Sci. **18**, 47.

Kee R.J., Rupley F.M., Miller J.A. (1989) CHEMKIN-II: A FORTRAN Chemical Kinetics Package for the Analysis of Gas-Phase Chemical Kinetics, SAND89-8009, Sandia National Laboratories: Albequerque, NM.

Kee R.J., Grcar J.F., Smooke M.D., Miller J.A. (1986a) A FORTRAN Program for Modeling Steady Laminar One-Dimensional Premixed Flames, SAND85-8240, Sandia National Laboratories: Albequerque, NM.

Kee R.J., Dixon-Lewis G., Warnatz J., Coltrin M.E., Miller J.A., (1986b) A FORTRAN Computer Code Package for the Evaluation of Gas-Phase Viscosities, Conductivities, and Diffusion Coefficients, SAND86-8246, Sandia National Laboratories: Albequerque, NM.

Lam S.H., Goussis D.A. (1988) Proc. Combust. Inst. **22**, 931.

Lam S.H., Goussis D.A. (1994) Int. J. Chem. Kinet. **26**, 461.

Law C.K., Sung C.J., Wang H., Lu T.F. (2003) AIAA J. **41**, 1629.

Lovas T., Nilsson D., Mauss F. (2000) Proc. Combust. Inst. **28**, 1809.

Lu T.F., Law C.K. (2005) Proc. Combust. Inst. **30**, 1333.

Lu T.F., Law C.K. (2006a) Combust. Flame **146**, 472.

Lu T.F., Law C.K. (2006b) Combust. Flame **144**, 24.

Lu T.F., Law C.K. (2008) Combust. Flame **154**, 761.

Lu T.F., Law C.K. (2009) Prog. Energy Combust. Sci. **35**, 192.

Lu T.F., Ju Y.G., Law C.K. (2001) Combust. Flame **126**, 1445.

Maas U., Pope S.B. (1992) Combust. Flame **88**, 239.

Massias A., Diamantis D., Mastorakos E., Goussis D.A. (1999a) Combust. Flame **117**, 685.

Massias A., Diamantis D., Mastorakos E., Goussis D.A. (1999b) Combust. Theory Model. **3**, 233.

Mendiara T., Alzueta M.U., Millera A., Bilbao R. (2004) Energy Fuel. **18**, 619.

Middha P., Wang H (2005) Combust. Theory Model. **9**, 353.

Montgomery C.J., Yang C.G., Parkinson A.R., Chen J.Y. (2006) Combust. Flame **144**, 37.

More J., Garbow B., Hillstrom K. (1999) Minpack. http://netlib.org/minpack/index.html, (March 6, 2012).

Pepiot-Desjardins P., Pitsch H. (2008) Combust. Flame **154**, 67.

Peters N., Williams F.A. (1987) Combust. Flame **68**, 185.

Rabitz H., Kramer M., Dacol D. (1983) Annu. Rev. Phys. Chem. **34**, 419.

Sankaran R., Hawkes E.R., Chen J.H., Lu T.F., Law C.K. (2007) Proc. Combust. Inst. **31**, 1291.

Sheen D.A., Wang H. (2011a) Combust. Flame **158**, 645.

Sheen D.A., Wang H. (2011b) Combust. Flame **158**, 2358.

Soyhan H.S., Mauss F., Sorusbay C. (2002) Combust. Sci. Technol. **174**, 73.

Sung C.J., Law C.K., Chen J.Y. (2001) Combust. Flame **125**, 906.

Tomlin A.S., Turanyi T., Pilling M.J. (1998) Mathematical Tools for Construction, Investigation and Reduction of Combustion Mechanisms; Elsevier.

Tomlin A.S., Turanyi T., Pilling M.J. (1997) Comprehensive Chemical Kinetics; Elsevier.

Turanyi T. (1990) J. Math. Chem. **5**, 203.

Turanyi T. (1990) New J. Chem. **14**, 795.

Valorani M., Najm H.N., Goussis D.A. (2003) Combust. Flame **134**, 35.

Valorani M., Creta F., Goussis D.A., Lee J.C., (2006) Combust. Flame **146**, 29.

Vajda S., Valko P., Turanyi T. (1985) Int. J. Chem. Kinet. **17**, 55.

Wang H., Frenklach M. (1991) Combust. Flame **87**, 365.

Wang H., You X.Q., Joshi A.V., Davis S.G., Laskin A., Egolfopoulos F., Law C.K. (2007) USC Mech Version II. High-Temperature Combustion Reaction Model of H2/CO/C1-C4 Compounds. http://ignis.usc.edu/USC_Mech_II.htm.

Westbrook C. K., Pitz W.J., Herbinet O., Curran H.J., Silke E.J. (2009) Combust. Flame **156**, 181.

Zheng X.L., Lu T.F., Law C.K. (2007) Proc. Combust. Inst. **31**, 367.